1   **Investigation of ordered mesoporous carbon potential as CO$_2$ adsorbent**

2   Gülce ÇAKMAN[1,*], Selim CEYLAN[1], Yıldıray TOPCU[1], Feza GEYİKÇİ[1]

3   *[1]Ondokuz Mayıs University, Faculty of Engineering, Department of Chemical Engineering, Atakum*
4   *55139, Samsun-TURKEY*
5   [*]gulce.cakman@omu.edu.tr

6   **Abstract**

7   In this study, an investigation was carried out in order to determine the potential of ordered mesoporous

8   carbon including high ratio sucrose in its composition as a CO$_2$ adsorbent. Structural characterizations of

9   silica and carbon material were determined by using a scanning electron microscope (SEM), N$_2$

10   adsorption/desorption and X-ray diffraction (XRD) analysis. CO$_2$ adsorption capacities of developed

11   adsorbent at various temperatures (25°C, 35°C and 50°C) were determined by using a thermogravimetric

12   analyzer under CO$_2$ flow. The maximum adsorption capacity was obtained as approximately 2.27 mmol g

13   CO$_2$ g^{-1} adsorbent which was remained almost the same in the desorption process. The first order reaction

14   kinetic model was well fitted with the experimental data. Arrhenius equation was used to calculate

15   activation energy which was obtained as -2.86 kJ mol^{-1} indicating barrier-less type adsorption. Results

16   showed that ordered mesoporous carbon could be a potential source for an efficient and low-cost

17   adsorbent for CO$_2$ capture.

18

19   **Keywords:** Ordered mesoporous carbon; CO$_2$ adsorption/desorption; kinetics

1. Introduction

In recent years, greenhouse gases have become one of the most concern issues [1]. The main factors of increasing greenhouse gas emission are economic and population growth. The environment has been affected negatively by the gas emissions such as increased global temperatures (0.12°C per decade since 1951), ocean acidification (26% increase in acidity since 1750), and rising average sea levels (0.19 m since 1901) [2]. At the same time, if it doesn't take precaution for this, it is estimated that the global temperature will increase by 1-5˚C in 2050 [3, 4]. One of the main components of greenhouse gases is CO_2 and it is significantly produced from anthropogenic sources and fossil fuel combustion [5, 6]. Also, it is reported that CO_2 contributes 60% of the total global warming caused by all greenscript gases [7]. For all these reasons, researchers pay attention to CO_2 capture. Solvent absorption, pressure and temperature swing adsorption, membrane separation and cryogenic distillation have also been used to capture CO_2 [8-10]. Nevertheless, some CO_2 capture processes have serious problems, such as energy penalties [11], economic and environmental drawbacks [12, 13] and amine waste during operation [14]. To overcome such problems, the development of solid adsorbents to CO_2 capture has come to the prominence [15]. A large variety of adsorbents may be used for CO_2 captures, such as zeolites, microporous silicates, aluminum phosphates, carbons, other porous oxides, metal-organic frameworks (MOFs), amine-grafted or impregnated silica [2, 16].

Solid adsorbents are very suitible for adsorption of CO_2 owing to high adsorption capacity, fast adsorption rate, and good stability [17]. One of the solid adsorbents is porous carbon materials have been attracting lots of awareness as potential large-scale adsorbents because of the many advantages such as well-ordered structure, high surface area, large tunable and uniform mesoporous size, high mechanical strength and good hydrothermal stability at extensive temperature ranges [18-21]. Carbons must have open pores to be accessible for the CO_2 molecules. Ryoo and co-workers [22] prepared a new family of mesoporous carbons to represent as the CMK series. These carbon materials have a well-ordered pore structure with the larger surface area [23]. All of this properties made CMK series excellent applicant for hydrogen storage, gas separation, electrochemistry, catalysis, and adsorption [24-26]. *Li and et al.* (2017) studied on CO_2 sorption over activated mesoporous carbon (AMC) and metal oxides (CeO_2, CuO, Mn_3O_4 and NiO) modified AMC with different pressure. The best result of CO_2 adsorption was 4.66 mmol/g at 273 K and 1 bar by using pure AMC as an adsorbent [27]. *Chomiak and et al.* (2017) investigated that

49   CO_2 adsorption on microporous granular activated carbons (GACs) that has been prepared by KOH

50   activation of walnut shell-based carbons. Carbons showed very high CO_2 adsorption, at 273 K up to 7.2

51   and 18.2 mmol/g under 1 and 30 bar, respectively[28]. *Ma et al.* (2018) studied CO_2 capture with

52   nanoporous carbons materials which was prepared by using a metal-organic framework (MOF-5) as a

53   template. The highest CO_2 adsorption capacity was obtained by nanoporous carbon that carbonized at

54   900˚C (3.70 mmol/g at 0˚C (1 atm)) [16]. In the study of *Pham et al.* (2016) nano-zeolite was evaluated

55   for its potential use in CO_2 capture via temperature swing adsorption. As a result of the experiments, the

56   best adsorption capacity of CO_2 by nano-zeolite was 4.81 mmol/g at a temperature of 20 °C and at a

57   pressure of 1 atm[8]. *Lashaki et al.* (2018) examined the impact of the support pore structure on the CO_2

58   adsorption performance of triamine-tethered SBA-15 silica. Large-pore supports exhibited the highest

59   surface density of amine groups (up to 35 μmol/m^2) and highest CO_2 uptakes (up to 1.88 mmol CO_2/g)

60   [2].

61   In most of the previous studies, adsorption isotherms of CO_2 adsorbents have been investigated and their

62   adsorption capacities have been examined by various characterizing technics. However, there are few

63   studies on CO_2 adsorption kinetics of such adsorbents. It is critical to examine adsorption kinetics, to

64   better understand the events that occur during the adsorbent-goal material reaction, and also to estimate

65   the time required to complete the adsorption process. Also, information on adsorbent characteristics and

66   reaction kinetics is important for proper adsorbent selection, reactor sizing and process optimization.

67   Thus, in this work we have carried out a comprehensive study both on CO_2 adsorption on to CMK-3

68   including characterization and kinetics.

69   In this study, it was carried out for the potential of the ordered mesoporous carbon to be used in carbon

70   dioxide removal. SBA-15 was used as a template to synthesize ordered mesoporous carbon material,

71   CMK-3, for CO_2 capture. Characterization of the adsorbent was carried out with different analytical

72   instruments such as BET (Brunauer–Emmett–Teller), SEM (Scanning Electron Microscope), XRD (X-ray

73   powder diffraction) and TGA (Thermogravimetric Analyzer). In addition, the mechanism of adsorption

74   reaction was investigated and related kinetic parameters were calculated.

75

76

77

78 **2.   Materials and Methods**

79 *2.1.   Materials*

80 Sucrose ($C_{12}H_{22}O_{11}$), pluronic 123 (P123), sulfuric acid (H_2SO_4) and hydrochloric acid (HCl) was

81 supplied by Sigma-Aldrich. Tetraethylorthosilicate (TEOS) was purchased from Sigma-Aldrich with 97%

82 purity. Hydrofluoric acid (HF) was supplied by Merck. The purity of hydrofluoric acid is 40%.

83 *2.2.   Synthesis of adsorbent*

84 SBA-15 was synthesized according to Zhao et al. (1998) [29]. For the synthesis of CMK-3, sucrose

85 ($C_{12}H_{22}O_{11}$), sulfuric acid and deionized water were used as a carbon source, acid solution, and solvent,

86 respectively. CMK-3 was synthesized according to Jun et al. (2000)[30]. In briefly, 1.25 g sucrose, 5 g of

87 deionized water and 0.14 g H_2SO_4 were stirred until a homogeneous solution was formed. 1 g of SBA-15

88 was added to this solution and continued to stir. The mixture was placed aged in a furnace at 100°C for 6

89 hours and the furnace temperature was increased to 160°C and maintained for 6 hours. 0.8 g sucrose, 0.08

90 g H_2SO_4 and 5 g of deionized water were added to this solution and were treated again for the same

91 process (step 2). The resulting material was milled and carbonized in an inert atmosphere at 900°C for 3

92 hours at 7°C/min as a heating rate. After carbonization, the material was washed with HF and ionized

93 water and dried overnight.

94 *2.3.   Characterization of adsorbent*

95 The surface area, pore size, pore size distribution and pore volume values of synthesis samples were

96 determined by using nitrogen adsorption/desorption isotherms. Nitrogen adsorption/desorption isotherms

97 were studied by using Quantachrome Corporation, Autosorb.

98 Silica and carbon structures were investigated to use STOE IPDS II Model X-ray diffraction device. X-

99 ray diffraction pattern of the synthesized sample, the step in the range of 0.02 and 0.025 (2θ/s) CuKα

100 beam having a wavelength of 0.15406 nm were obtained. The characteristic peaks of silica and carbon

101 were determined at 2θ between 1°-10°. Unit cell parameter (a_0), d100 spacing values (d_{100}) and pore wall

102 thickness (δ) for SBA-15 and CMK-3 were calculated by using equation (1), equation (2) and equation

103 (3), respectively. In equation (3), dp is pore diameter which is calculated by using the BJH method.

104 $$d_{100} = \frac{n\lambda}{2sin\theta} \qquad\qquad (1)$$

105      $a_0 = \frac{2d100}{\sqrt{3}}$ **(2)**

106      $\delta = a - 0{,}95 \times dp$ **(3)**

107 The morphologies of all the materials were observed using a scanning electron microscopy (SEM). The

108 surfaces of silica structures were plated with a thin layer of gold-palladium before inspection under SEM.

109 The SEM analysis was conducted with JEOL JSM-7001FTTLS LV SEM machine.

110 *2.4. CO_2 adsorption experiments*

111 CO_2 adsorption capacity was determined by DTA-TG Analysis unit (Shimadzu, Japan) (Creamer et al.,

112 2016). A sample weight of carbon approximately 20 mg was placed into an alumina sample pan. The

113 placed sample was dried at 393 K for 1 h in a nitrogen atmosphere to potential volatile components out of

114 the sample and then cooled down to room temperature. Nitrogen gas flow rate was 50 mL/min for both

115 heating and cooling. When the system was at equilibrium, the CO_2 gas stream was switched on at a rate of

116 50 mL/min for 3 h. The adsorption capacity in percent was computed from the weight change of the

117 sample in the TG adsorption process.

118 *2.5.   Kinetic studies*

119 The CO_2 adsorption kinetics onto carbon adsorbent can be described using various kinetic model such as

120 pseudo-first order (Eq. 4) and pseudo-second order (Eq. 5) model [31].

121      $\dfrac{dq_t}{dt} = k_1 \times (q_e - q_t)$ **(4)**

122      $\dfrac{dq_t}{dt} = k_2 \times (q_e - q_t)^2$ **(5)**

123 Where q_t (mg g^{-1}) and q_e (mg g^{-1}) are the concentrations of CO_2 adsorption at time *t* and at equilibrium,

124 respectively, k_1 and k_2 (g mg^{-1} s^{-1}) is the first and second-order adsorption rate constants.

125 The activation energy must be minimum value in order to facilitate the adsorption process. The activation

126 energy can be calculated using the Arrhenius equation shown in Equation (6) [32].

127      $\ln k = \ln A - \dfrac{E_a}{RT}$ **(6)**

128 According to Equation (6), k_1 is the rate constant, A is the temperature impact factor, E_a is the activation

129 energy for adsorption (J/mol), R is the gas constant (8.314 J/mol K) and T is the adsorption temperature in

130 K.

131 **3.   Result and Discussion**

132 *3.1.   Characterizations of carbon materials*

133 The ordered pore structure, surface area and morphological structure of the synthesized adsorbent were

134 determined by XRD, nitrogen adsorption/desorption isotherm and SEM, respectively.

135

136 *3.1.1. N_2 adsorption/desorption*

137 The textural parameters of SBA-15 and CMK-3 samples are investigated using N_2 adsorption/desorption

138 technique. The textural parameters of these samples including the specific surface area, specific pore

139 volume, and average pore size are summarized in Table 1. The specific surface area and total pore volume

140 of the CMK-3 are 1360 m^2/g and 1.167 cm^3/g, respectively. These results are consistent with the literature

141 [1, 33].

142 Figure 1 shows the N_2 adsorption/desorption isotherms and pore distributions of samples. The synthesized

143 SBA-15 and CMK-3 have been shown to exhibit Type IV isotherm behavior in the BDDT (Brunauer-

144 Deming-Deming-Teller) classification as in the literature [34, 35]. According to Figure 1.a, SBA-15 and

145 CMK-3 samples prove to have a mesopore structure. It also shows that in addition to mesoporosity, the

146 structures also have microporosity. From the adsorption/desorption isotherms, the hysteresis loop for the

147 SBA-15 and CMK-3 samples are observed at partial pressure values in the range of 0.65-0.80 and 0.45-

148 0.6 for P/P_0, respectively. This type of hysteresis (H1 hysteresis) shows that the structure has a cylindrical

149 structure [36]. The sharp increase and decrease in the hysteresis region is indicative of the narrow pore

150 size distribution in accordance with the pore size distribution shown in Figure 1b. The pore size

151 distributions shown in Figure 1.b are performed by the BJH method for mesopore and SF method for

152 micropore. The average pore size of CMK-3 is 2.03 nm.

153 *3.1.2 Small Angle X-Ray Diffraction*

154 Figure 2 shows the small angle powder XRD patterns of SBA-15 and CMK-3 samples. The SAXS

155 patterns of SBA-15 show the dominant signal peak corresponding to the (100) plane and two small

156 diffraction peaks at higher angles (110) and (200) plane, characteristic of a well-defined hexagonal 2D

157 structures of P6mm symmetry [37, 38]. CMK-3 was obtained from pore filling of SBA-15 and uniform

158 hexagonal carbon rods were formed. The CMK-3 sample provides a diffractogram with a dominant peak

159 corresponding to the (100) plane, characteristic of these kinds of ordered mesoporous carbons [39]. This

160 shows that CMK-3 succesfully replicate SBA-15 templates. The patterns for both SBA-15 and CMK-3

161 indicate that they are ordered mesoporous materials with well-defined pore geometry.

162 Unit cell parameter (a_0), d100 spacing values (d100) and pore wall thickness (δ) of all materials are given

163 in Table 2. The wall thickness of the SBA-15 and CMK-3 sample was calculated at 8.91 nm and 10.38

164 nm, respectively. It was found to be consistent with the wall thickness (3-9 nm) specified in the literature

165 [29, 40].

166 *3.1.3. SEM images*

167 The morphology of SBA-15 and CMK-3 are illustrated in Figure 3. SBA-15 structures are formed

168 homogeneously. SEM images have proven that CMK-3 is synthesized without change of the surface

169 morphology of SBA-15. SBA-15 and CMK-3 structures have rod-type morphology. The obtained SEM

170 images of SBA-15 and CMK-3 are good agreement with literature [41, 42]. EDX analysis of these

171 materials shows that the template has only silica for SBA-15 and the CMK-3 sample has only carbon,

172 confirming the success of the synthesis.

173 *3.2. Kinetic studies of CO_2 adsorption on the carbon material*

174 The TGA data on the CO_2 adsorption capacity of CMK-3 at 25˚C, 35 ˚C and 50 ˚C are shown in Figure 4.

175 It has been found that different CO_2 adsorption capacities at various temperatures. Because of CO_2

176 adsorption is an exothermic reaction, lower temperature is most suitable for CO_2 adsorption, The highest

177 adsorption capacity is obtained at 25˚C as approximately 2.27 mmol CO_2/g adsorbent. This indicates that

178 the higher driving force at 25˚C. As seen from Table 3, the adsorption capacity of the produced adsorbent

179 is within the range of previously reported ones. Thus it can be said that this type of adsorbent have a

180 potential for CO_2 capture processes.

181 CO_2 adsorption kinetics is determined by using different adsorption kinetic models such as pseudo-first-

182 order and pseudo-second-order. The pseudo-second-order model poorly fits into the kinetic data in which

183 low R^2 values were obtained. For this reason, the pseudo-first-order model can describe the adsorption

184   process of CO_2 on carbon adsorbent. Kinetic parameters at various temperatures are given in Figure 5a.

185   Pseudo-first order fits the CO_2 adsorption at all temperatures with high regression coefficient values

186   (>0.90). With the increase in temperature, decrease in rate constant which indicates an exothermic

187   process. The rate constant at 25˚C, 35˚C and 50˚C are 0.0030103 s^{-1}, 0.0028958 s^{-1} and 0.0027798 s^{-1},

188   respectively.

189   The *lnk* has been plotted versus the inverse of temperature (1/T) to determining the activation energy at

190   Figure 5b. The value of activation energy is found -2.86 kJ/mol. The activation energy is negative

191   because the reaction rate decreases as the temperature increases. CO_2 adsorption with negative activation

192   energy is categorized as barrier-less adsorption. This adsorption process depends on the capture of CO_2

193   molecules in a potential well.

219   In this case, the probability of collision of CO_2 molecules decreases as the temperature increases [43].

220   The activation energy value of different adsorbents is given in Table 4. The activation energy of CMK-3

221   for CO_2 adsorption showed similarity with literature.

222

223   *3.3. CO_2 Desorption on the carbon material*

224   Reusability is one of the most important parameters for adsorbents. For this reason, the reusability of

225   CMK-3 for CO_2 adsorption is also studied at 25˚C. Desorption process carried out an inert atmosphere

226   (N_2 flow) after CO_2 adsorption. This adsorption/desorption cycle was repeated two times and

227   distinguished variety are not observed in the CO_2 desorption or adsorption. As seen in Figure 6, similar

228   curves for both fresh and regenerated adsorbents and this indicates that the CO_2 adsorption capacity is the

229   almost the same. Therefore, CMK-3 can be reported as fast, easily, and completely regenerated over

230   multiple cycles without noticeable loss of adsorption capacity.

231   **4.   Conclusion**

232   In this study, CMK-3 has been synthesized and characterized in order to evaluate the potential of ordered

233   mesoporous carbon as a CO_2 adsorbent. According to the characterization, CMK-3 was succesfully

234   synthesis from pore filling of SBA-15. The adsorption capacity reduced with increase in temperature. The

235   highest adsorption capacity is obtained at 25˚C as approximately 2.27 mmol CO_2/g adsorbent. Kinetic

236   parameters were evaluated with pseudo-first order kinetics where a negative value of activation energy

237   obtained indicating barrier-less type CO_2 capture process. The desorption performance of the adsorbent

238   was almost same the adsorption capacity. Results showed that ordered mesoporous carbon, CMK-3, has

239   a potential in efficient CO_2 adsorbent.

240   **Acknowledgment**

243

244   **References**

245   [1] C.-C. Huang, S.-C. Shen, Adsorption of CO2 on chitosan modified CMK-3 at ambient temperature,
246   Journal of the Taiwan Institute of Chemical Engineers, 44 (2013) 89-94.
247   [2] M.J. Lashaki, A. Sayari, CO2 capture using triamine-grafted SBA-15: The impact of the support pore
248   structure, Chemical Engineering Journal, 334 (2018) 1260-1269.
249   [3] X. Liu, X. Zhai, D. Liu, Y. Sun, Different CO2 absorbents-modified SBA-15 sorbent for highly
250   selective CO2 capture, Chemical Physics Letters, 676 (2017) 53-57.
251   [4] P. Villoria-Saez, V.W. Tam, M. del Río Merino, C.V. Arrebola, X. Wang, Effectiveness of
252   greenhouse-gas Emission Trading Schemes implementation: a review on legislations, Journal of cleaner
253   production, 127 (2016) 49-58.
254   [5] A.E. Creamer, B. Gao, S. Wang, Carbon dioxide capture using various metal oxyhydroxide–biochar
255   composites, Chemical Engineering Journal, 283 (2016) 826-832.
256   [6] H.-K. Youn, J. Kim, G. Chandrasekar, H. Jin, W.-S. Ahn, High pressure carbon dioxide adsorption on
257   nanoporous carbons prepared by Zeolite Y templating, Materials Letters, 65 (2011) 1772-1774.
258   [7] K.S. Lakhi, W.S. Cha, J.-H. Choy, M. Al-Ejji, A.M. Abdullah, A.M. Al-Enizi, A. Vinu, Synthesis of
259   mesoporous carbons with controlled morphology and pore diameters from SBA-15 prepared through the
260   microwave-assisted process and their CO2 adsorption capacity, Microporous and Mesoporous Materials,
261   233 (2016) 44-52.
262   [8] T.-H. Pham, B.-K. Lee, J. Kim, C.-h. Lee, Enhancement of CO2 capture by using synthesized nano-
263   zeolite, Journal of the Taiwan Institute of Chemical Engineers, 64 (2016) 220-226.
264   [9] A. Huang, L.-H. Chen, C.-H. Chen, H.-Y. Tsai, K.-L. Tung, Carbon dioxide capture using an
265   omniphobic membrane for a gas-liquid contacting process, Journal of Membrane Science, 556 (2018)
266   227-237.
267   [10] A.M. Yousef, W.M. El-Maghlany, Y.A. Eldrainy, A. Attia, New Approach for Biogas Purification
268   using Cryogenic Separation and Distillation Process for CO 2 Capture, Energy, (2018).
269   [11] A. Padurean, C.-C. Cormos, P. Şerban Agachi, TECHNO-ECONOMICAL EVALUATION OF
270   POST-AND PRE-COMBUSTION CARBON DIOXIDE CAPTURE METHODS APPLIED FOR AN
271   IGCC POWER GENERATION PLANT, Environmental Engineering & Management Journal (EEMJ), 12
272   (2013).
273   [12] Y. Jing, L. Wei, Y. Wang, Y. Yu, Synthesis, characterization and CO2 capture of mesoporous SBA-
274   15 adsorbents functionalized with melamine-based and acrylate-based amine dendrimers, Microporous
275   and Mesoporous Materials, 183 (2014) 124-133.
276   [13] R. Ullah, M. Atilhan, S. Aparicio, A. Canlier, C.T. Yavuz, Insights of CO2 adsorption performance
277   of amine impregnated mesoporous silica (SBA-15) at wide range pressure and temperature conditions,
278   International Journal of Greenhouse Gas Control, 43 (2015) 22-32.
279   [14] G.T. Rochelle, Amine scrubbing for CO2 capture, Science, 325 (2009) 1652-1654.
280   [15] T.C. Drage, C.E. Snape, L.A. Stevens, J. Wood, J. Wang, A.I. Cooper, R. Dawson, X. Guo, C.
281   Satterley, R. Irons, Materials challenges for the development of solid sorbents for post-combustion carbon
282   capture, Journal of Materials Chemistry, 22 (2012) 2815-2823.
283   [16] X. Ma, L. Li, R. Chen, C. Wang, H. Li, S. Wang, Heteroatom-doped nanoporous carbon derived
284   from MOF-5 for CO2 capture, Applied Surface Science, 435 (2018) 494-502.
285   [17] Y. Liu, X. Lin, X. Wu, M. Liu, R. Shi, X. Yu, Pentaethylenehexamine loaded SBA-16 for CO2
286   capture from simulated flue gas, Powder Technology, 318 (2017) 186-192.
287   [18] Y. Zhao, L. Zhao, K.X. Yao, Y. Yang, Q. Zhang, Y. Han, Novel porous carbon materials with
288   ultrahigh nitrogen contents for selective CO 2 capture, Journal of Materials Chemistry, 22 (2012) 19726-
289   19731.
290   [19] Q.-F. Deng, L. Liu, X.-Z. Lin, G. Du, Y. Liu, Z.-Y. Yuan, Synthesis and CO2 capture properties of
291   mesoporous carbon nitride materials, Chemical engineering journal, 203 (2012) 63-70.
292   [20] G. Singh, K.S. Lakhi, K. Ramadass, S. Kim, D. Stockdale, A. Vinu, A combined strategy of acid-
293   assisted polymerization and solid state activation to synthesize functionalized nanoporous activated
294   biocarbons from biomass for CO 2 capture, Microporous and Mesoporous Materials, 271 (2018) 23-32.
295   [21] Y. Liu, Y. Chen, L. Tian, R. Hu, Hierarchical porous nitrogen-doped carbon materials derived from
296   one-step carbonization of polyimide for efficient CO 2 adsorption and separation, Journal of Porous
297   Materials, 24 (2017) 583-589.
298   [22] R. Ryoo, S.H. Joo, S. Jun, Synthesis of highly ordered carbon molecular sieves via template-
299   mediated structural transformation, The Journal of Physical Chemistry B, 103 (1999) 7743-7746.

10

[23] G. Chandrasekar, W.-J. Son, W.-S. Ahn, Synthesis of mesoporous materials SBA-15 and CMK-3 from fly ash and their application for CO 2 adsorption, Journal of porous materials, 16 (2009) 545-551.

[24] J.M. Juárez, B.C. Ledesma, M.G. Costa, A.R. Beltramone, O.A. Anunziata, Novel preparation of CMK-3 nanostructured material modified with titania applied in hydrogen uptake and storage, Microporous and Mesoporous Materials, 254 (2017) 146-152.

[25] Y. Yang, J. Wang, X. Qian, Y. Shan, H. Zhang, Aminopropyl-functionalized mesoporous carbon (APTMS-CMK-3) as effective phosphate adsorbent, Applied Surface Science, 427 (2018) 206-214.

[26] Y. Xu, Y. Li, C. Wang, C. Wang, L. Ma, T. Wang, X. Zhang, Q. Zhang, In-situ hydrogenation of model compounds and raw bio-oil over Ni/CMK-3 catalyst, Fuel Processing Technology, 161 (2017) 226-231.

[27] M. Li, K. Huang, J.A. Schott, Z. Wu, S. Dai, Effect of metal oxides modification on CO 2 adsorption performance over mesoporous carbon, Microporous and Mesoporous Materials, 249 (2017) 34-41.

[28] K. Chomiak, S. Gryglewicz, K. Kierzek, J. Machnikowski, Optimizing the properties of granular walnut-shell based KOH activated carbons for carbon dioxide adsorption, Journal of CO2 Utilization, 21 (2017) 436-443.

[29] D. Zhao, J. Feng, Q. Huo, N. Melosh, G.H. Fredrickson, B.F. Chmelka, G.D. Stucky, Triblock copolymer syntheses of mesoporous silica with periodic 50 to 300 angstrom pores, science, 279 (1998) 548-552.

[30] S. Jun, S.H. Joo, R. Ryoo, M. Kruk, M. Jaroniec, Z. Liu, T. Ohsuna, O. Terasaki, Synthesis of new, nanoporous carbon with hexagonally ordered mesostructure, Journal of the American Chemical Society, 122 (2000) 10712-10713.

[31] J.-P. Simonin, On the comparison of pseudo-first order and pseudo-second order rate laws in the modeling of adsorption kinetics, Chemical Engineering Journal, 300 (2016) 254-263.

[32] M.S.R. Shahrom, C.D. Wilfred, F.K. Chong, Thermodynamic and kinetic studies on CO2 capture with Poly [VBTMA][Arg], Journal of Physics and Chemistry of Solids, 116 (2018) 22-29.

[33] K. Ghani, N. Kiomarsipour, H. Jaberi, Evaluation of optical properties of CMK-1 and CMK-3 mesoporous carbons and introduction them as very interesting black pigments, Dyes and Pigments, 122 (2015) 126-133.

[34] M. Araujo, L. Silva, J. Sczancoski, M. Orlandi, E. Longo, A. Santos, J. Sa, R. Santos, G. Luz Jr, L. Cavalcante, Anatase TiO2 nanocrystals anchored at inside of SBA-15 mesopores and their optical behavior, Applied Surface Science, 389 (2016) 1137-1147.

[35] W. Tang, Y. Deng, Y. Chen, Promoting effect of acid treatment on Pd-Ni/SBA-15 catalyst for complete oxidation of gaseous benzene, Catalysis Communications, 89 (2017) 86-90.

[36] Z.A. ALOthman, A review: fundamental aspects of silicate mesoporous materials, Materials, 5 (2012) 2874-2902.

[37] S. Sareen, V. Mutreja, S. Singh, B. Pal, Fine CuO anisotropic nanoparticles supported on mesoporous SBA-15 for selective hydrogenation of nitroaromatics, Journal of colloid and interface science, 461 (2016) 203-210.

[38] C. Ochoa-Hernández, Y. Yang, P. Pizarro, A. Víctor, J.M. Coronado, D.P. Serrano, Hydrocarbons production through hydrotreating of methyl esters over Ni and Co supported on SBA-15 and Al-SBA-15, Catalysis today, 210 (2013) 81-88.

[39] S.H. Joo, R. Ryoo, M. Kruk, M. Jaroniec, Evidence for general nature of pore interconnectivity in 2-dimensional hexagonal mesoporous silicas prepared using block copolymer templates, The Journal of Physical Chemistry B, 106 (2002) 4640-4646.

[40] V. Meynen, P. Cool, E.F. Vansant, Verified syntheses of mesoporous materials, Microporous and mesoporous materials, 125 (2009) 170-223.

[41] R. Radhakrishnan, S. Thiripuranthagan, A. Devarajan, S. Kumaravel, E. Erusappan, K. Kannan, Oxidative esterification of furfural by Au nanoparticles supported CMK-3 mesoporous catalysts, Applied Catalysis A: General, 545 (2017) 33-43.

[42] G. Zhu, L. Wang, Y. Zhang, W. Yu, H. Xie, Au–Ag alloy nanoparticles supported on ordered mesoporous carbon (CMK-3) with remarkable solar thermal conversion efficiency, Applied Physics A, 125 (2019) 151.

[43] Q. Liu, J. Shi, S. Zheng, M. Tao, Y. He, Y. Shi, Kinetics studies of CO2 adsorption/desorption on amine-functionalized multiwalled carbon nanotubes, Industrial & Engineering Chemistry Research, 53 (2014) 11677-11683.

[44] X. Wu, M. Liu, R. Shi, X. Yu, Y. Liu, CO 2 adsorption/regeneration kinetics and regeneration properties of amine functionalized SBA-16, Journal of Porous Materials, 1-9.

357 [45] D. Tiwari, S. Kaur, H. Bhunia, P.K. Bajpai, CO_2 adsorption on oxygen enriched nanostructured
358 carbons derived from silica templated resorcinol-formaldehyde, Journal of Industrial and Engineering
359 Chemistry, (2018).
360 [46] K. Kamarudin, N. Zaini, N. Khairuddin, CO_2 removal using amine-functionalized kenaf in pressure
361 swing adsorption system, Journal of environmental chemical engineering, 6 (2018) 549-559.
362 [47] N.S. Nasri, U.D. Hamza, S.N. Ismail, M.M. Ahmed, R. Mohsin, Assessment of porous carbons
363 derived from sustainable palm solid waste for carbon dioxide capture, Journal of cleaner production, 71
364 (2014) 148-157.
365 [48] M. Wei, Q. Yu, H. Xie, Z. Zuo, L. Hou, F. Yang, Kinetics studies of CO_2 adsorption and desorption
366 on waste ion-exchange resin-based activated carbon, International Journal of Hydrogen Energy, 42 (2017)
367 27122-27129.
368 [49] S.N. Kudahi, A.R. Noorpoor, N.M. Mahmoodi, Determination and analysis of CO_2 capture kinetics
369 and mechanisms on the novel graphene-based adsorbents, Journal of CO_2 Utilization, 21 (2017) 17-29.
370 [50] Y. Liu, X. Yu, Carbon dioxide adsorption properties and adsorption/desorption kinetics of amine-
371 functionalized KIT-6, Applied Energy, 211 (2018) 1080-1088.

372

373   **Table List**

374   **Table 1** Textural properties of SBA-15 and CMK-3

375   **Table 2** Unit cell parameter (a_0), d100 spacing values (d100) and pore wall thickness (δ)

376   **Table 3** Comparison of adsorption capacities

377   **Table 4** Activation energy of CO_2 adsorption for various adsorbent

378 **Table 1** Textural property of SBA-15 and CMK-3

Adsorbents	BET Surface Area (m^2/g)	Total Pore Volume (cm^3/g)	BJH Method Average Pore Size (nm)	SF Method Average Pore Size (nm)
SBA-15	753	1.285	3.9	0.47
CMK-3	1360	1.167	2.03	0.46

379

380 **Table 2.** Unit cell parameter (a_0), d100 spacing values (d100) and pore wall thickness(δ)

Adsorbents	d (nm)	a (nm)	δ (nm)
SBA-15	10.63	12.61	8.91
CMK-3	10.64	12.28	10.38

381

382 **Table 3.** Comparison of adsorption capacities with literature

Material	Condition	Capacity (mmol/g)	Reference
Activated carbon	273 K and 1 bar	4.66	[27]
PEHA-loaded SBA-16	343 K and 1 atm	2.1	[44]
KOH activated walnut shell-based carbons	273 K and 1 bar	7.2	[28]
Metal-organic framework	273 K and 1 atm	3.70	[16]
Nano zeolite	293 K and 1 atm	4.81	[8]
Nano structured carbon	303 K and 1 atm	1.5	[45]
Amine activated kenaf		2.086	[46]
Palm activated char	303 K and 1 bar	1.66	[47]
Al salt activated cottonwood	298 K and 1 bar	1.61	[5]
CMK-3	298 K and 1 atm	2.27	*This study*

383

384

385 **Table 4** Activation energy of CO_2 adsorption for various adsorbent

Adsorbent	Activation Energy (kJ/mol)	References
Activated Carbon	-2.28	[48]
Thermally treated graphene nanosheets	-7.21	[49]
Amine functionalized KIT-6*	-6.56	[50]
CMK-3	-2.86	In this study

386 * CO_2 concentration (vol %60)

387 **Figure List**

388 **Figure 1 (a)** N_2 adsorption/desorption isotherms **(b)** Pore distributions of SBA-15 and CMK3

389 **Figure 2** XRD Patterns of SBA-15 and CMK-3

390 **Figure 3** SEM images of (a) SBA-15 and (b) CMK-3

391 **Figure 4** CO_2 adsorption capacity of CMK-3 at various temperatures

392 **Figure 5 a)** Kinetic plot of pseudo first order model with various temperatures **b)** Arrhenius plot for

393 activation energy calculation

394 **Figure 6** CO_2 adsorption and desorption capacity of CMK-3
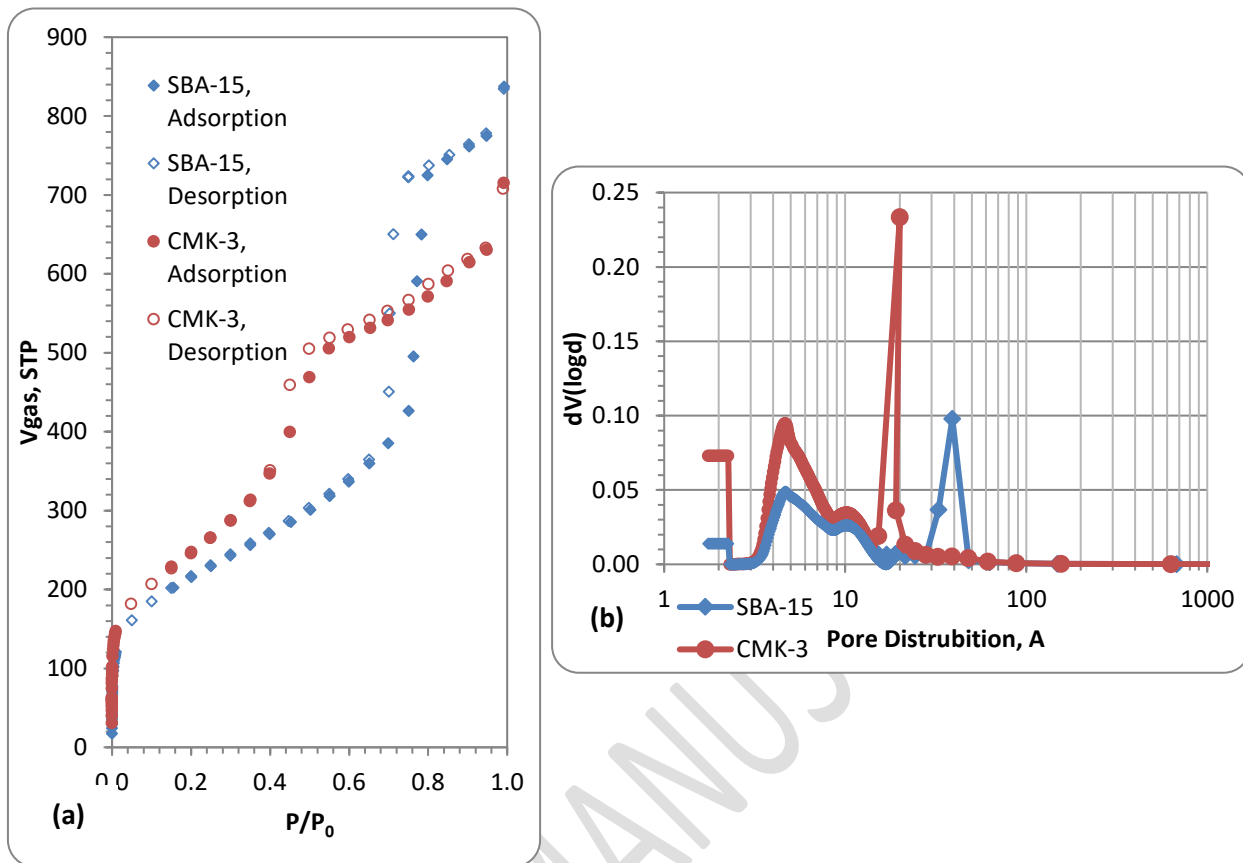
Figure 1 (**a**) N_2 adsorption/desorption isotherms (**b**) Pore distributions of SBA-15 and CMK-3
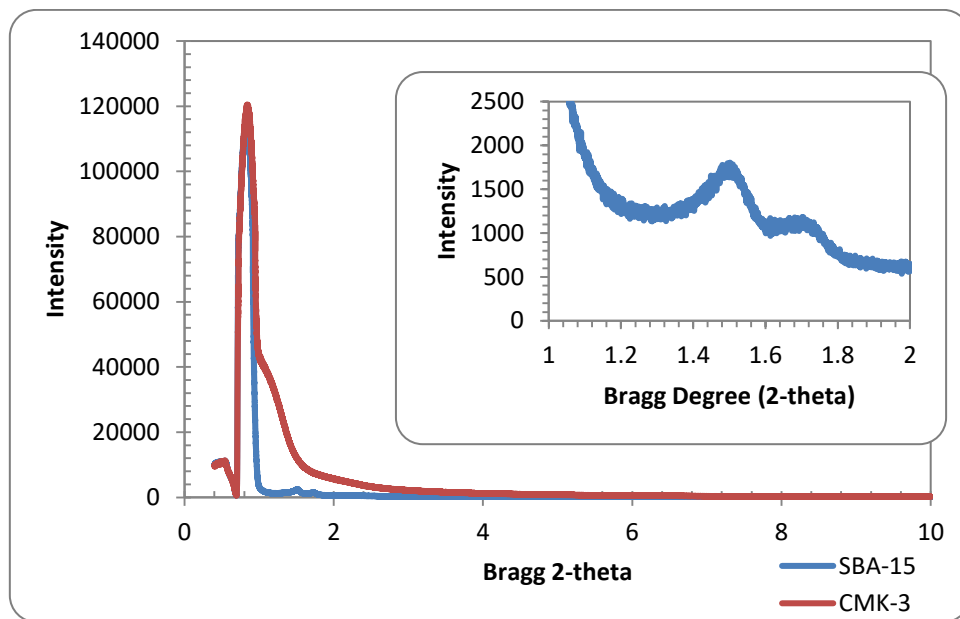
400

401 **Figure 2** XRD Patterns of SBA-15 and CMK-3
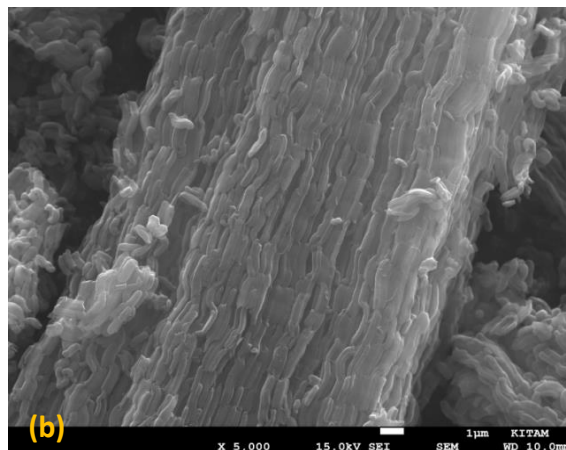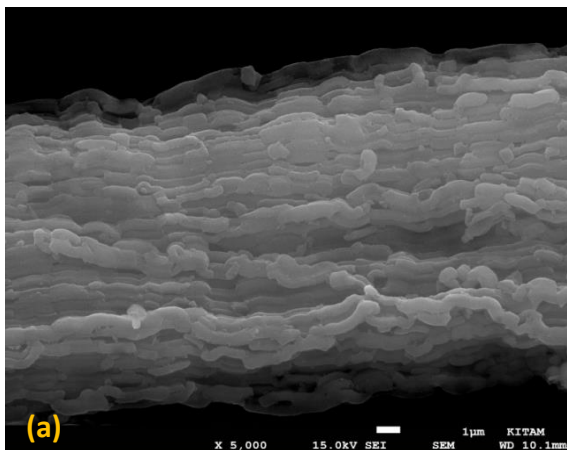
402

403   **Figure 3** SEM images of (a) SBA-15 and (b) CMK-3

404
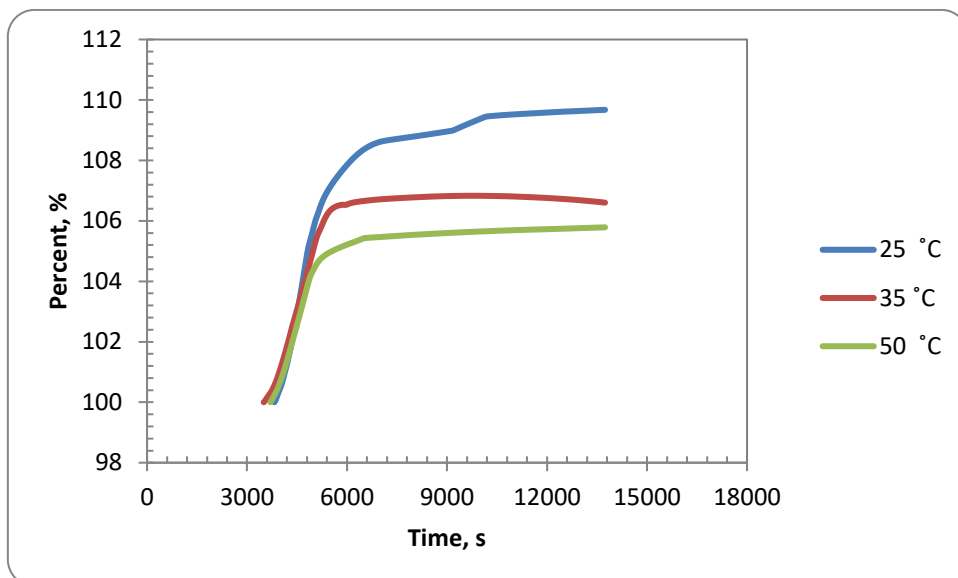
Figure 4 CO_2 adsorption capacity of CMK-3 with various temperatures

405

406   **a)**

407   **b)**
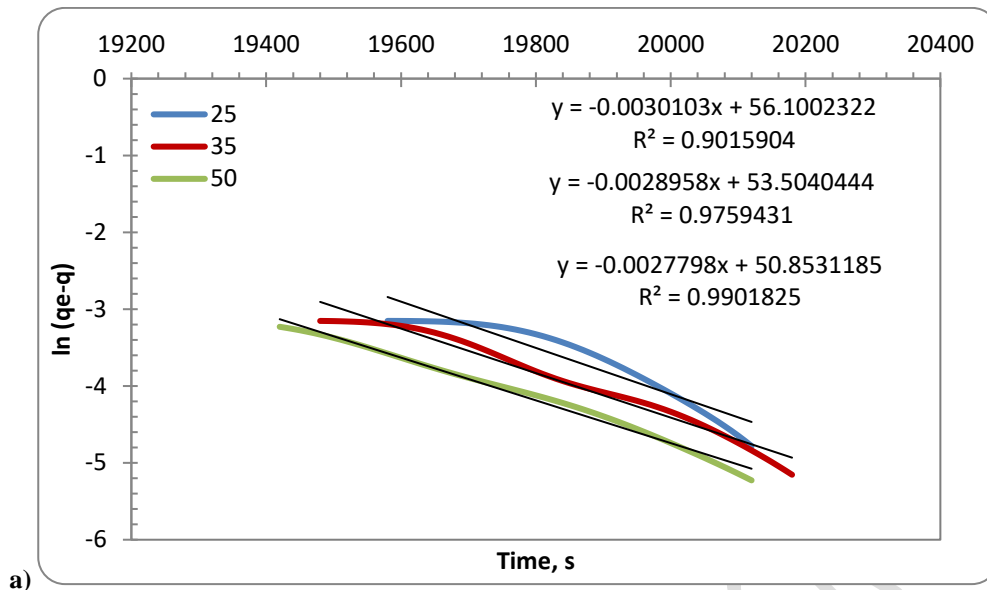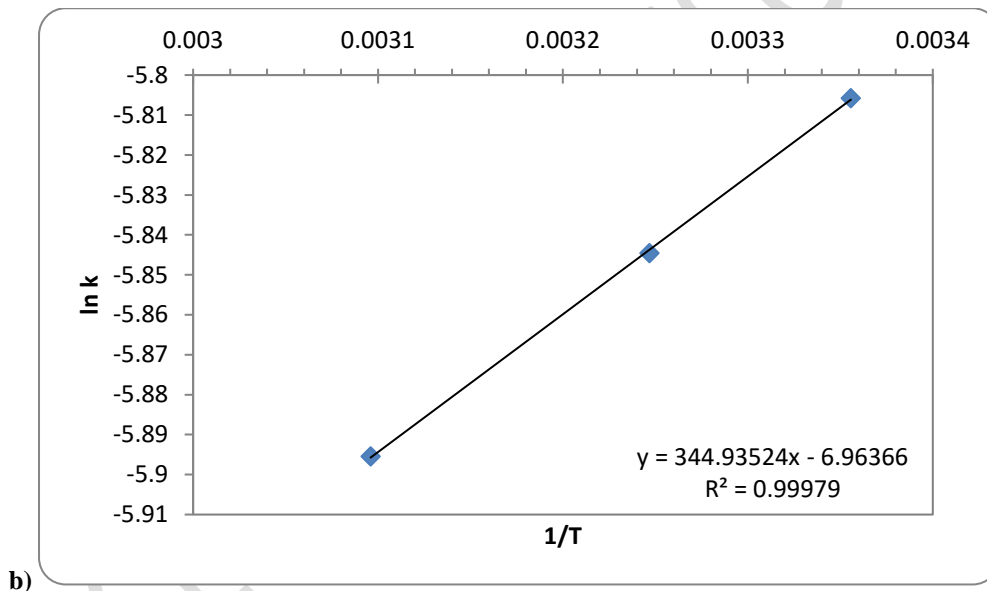
408   **Figure 5 a)** Kinetic plot of pseudo first order model with various temperatures **b)** Arrhenius plot for

409   activation energy calculation

410
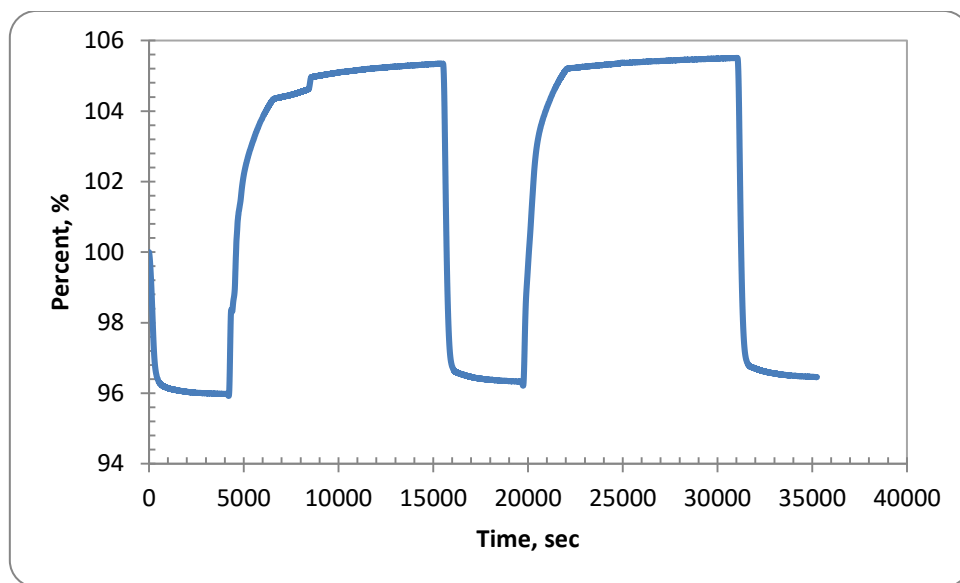
411

412 **Figure 6** CO_2 adsorption and desorption capacity of CMK-3